NANO LETTERS
Cite This: Nano Lett. 2019, 19, 5653−5660
Letter
pubs.acs.org/NanoLett

Plasmon-Mediated Synthesis of Periodic Arrays of Gold Nanoplates Using Substrate-Immobilized Seeds Lined with Planar Defects

Spencer D. Golze,[†] Robert A. Hughes,[†] Sergei Rouvimov,[‡] Robert D. Neal,[†] Trevor B. Demille,[†] and Svetlana Neretina*[,†,§]

[†]College of Engineering, [‡]Notre Dame Integrated Imaging Facility, and [§]Department of Chemistry and Biochemistry, University of Notre Dame, Notre Dame, Indiana 46556, United States

Supporting Information

ABSTRACT: The seed-mediated growth of noble metal nanostructures with planar geometries requires the use of seeds lined with parallel stacking faults so as to provide a break in symmetry in an otherwise isotropic metal. Although such seeds are now routinely synthesized using colloidal pathways, equivalent pathways have not yet been reported for the fabrication of substrate-based seeds with the same internal defect structures. The challenge is not merely to form seeds with planar defects but to do so in a deterministic manner so as to have stacking faults that only run parallel to the substrate surface while still allowing for the lithographic processes needed to regulate the placement of seeds. Here, we demonstrate substrate-imposed epitaxy as a viable synthetic control able to induce planar defects in Au seeds while simultaneously dictating nanostructure in-plane alignment and crystallographic orientation. The seeds, which are formed in periodic arrays using nanoimprint lithography in combination with a vapor-phase assembly process, are subjected to a liquid-phase plasmon-mediated synthesis that uses light as an external stimuli to drive a reaction yielding periodic arrays of hexagonal Au nanoplates. These achievements not only represent the first of their kind demonstrations but also advance the possibility of integrating wafer-based technologies with a rich and exciting nanoplate colloidal chemistry.

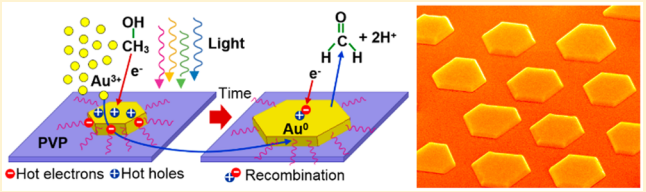

KEYWORDS: *Nanoplate, nanoprism, plasmon-mediated, stacking fault, twin boundary, seed-mediated*

Plasmon-mediated syntheses represent a distinct branch of photochemistry in which short-lived plasmonic excitations act as the primary driver for a redox chemistry yielding highly faceted nanostructures.[1−4] Mirkin and co-workers[5] were the first to demonstrate that citrate-protected colloidal Ag nanospheres, when illuminated with a fluorescent light source, are transformed into a monodisperse population of triangular nanoprisms. The discovery not only opened the door to a new photochemistry but represented a significant advance in that it was the first synthesis to realize plasmonic nanoplates in high yield. This demonstration was followed by a series of reports that forwarded a mechanistic understanding of the growth mode.[6−11] One of the quandaries faced was that the plasmon-mediated growth seemed limited to Ag. This elemental exclusivity was, however, recently overcome by Wei and co-workers[12] who demonstrated the synthesis of single-crystal Au nanoplates with triangular and hexagonal geometries using a plasmon-mediated chemistry.

With the vast majority of plasmonically driven growth modes being seed-mediated, it has become apparent that the decisive factor in determining the nanostructure shape is the internal defect structure of the seed.[1,2] While singly twinned and multitwinned (e.g., icosahedral, decahedral) seeds have been used to generate some of the most intricate nanostructure architectures,[13−15] it is seeds lined with parallel planar defects that are most closely connected to the nanoplate geometry.[1,2,13] Planar defects, which in face-centered cubic (fcc) metals manifest themselves as deviations from the ABCABC··· stacking order along ⟨111⟩-axes, can take the form of an added or missing row or a twin defect where the stacking order is reversed at a mirror plane (i.e., ABC|A|CBA where |A| is the mirror plane). The roles played by such defects are to (i) provide a symmetry-breaking structure with a two-dimensional character in an otherwise isotropic metal, (ii) create high surface energy sites conducive to the reduction of metal ions, and (iii) facilitate the selective adsorption of suitably chosen capping agents. These mechanistic roles are not limited to plasmon-driven syntheses, as they apply equally to thermally driven growth modes yielding planar architectures.[16−20]

Although the synthesis and application of plasmonic nanoplates as colloids has been an unmitigated success, it has proven quite challenging to form organized surfaces of such structures on planar substrates using the same solution-based chemistry. Obtaining close packed arrangements of nanoplates over large areas using self-assembly is inherently difficult and although progress has been made,[21,22] long-range order has not yet been achieved. Although numerous examples exist where colloidal seeds have been dispersed onto substrates

Received: May 30, 2019
Revised: July 8, 2019
Published: July 31, 2019

DOI: 10.1021/acs.nanolett.9b02215
Nano Lett. 2019, 19, 5653−5660

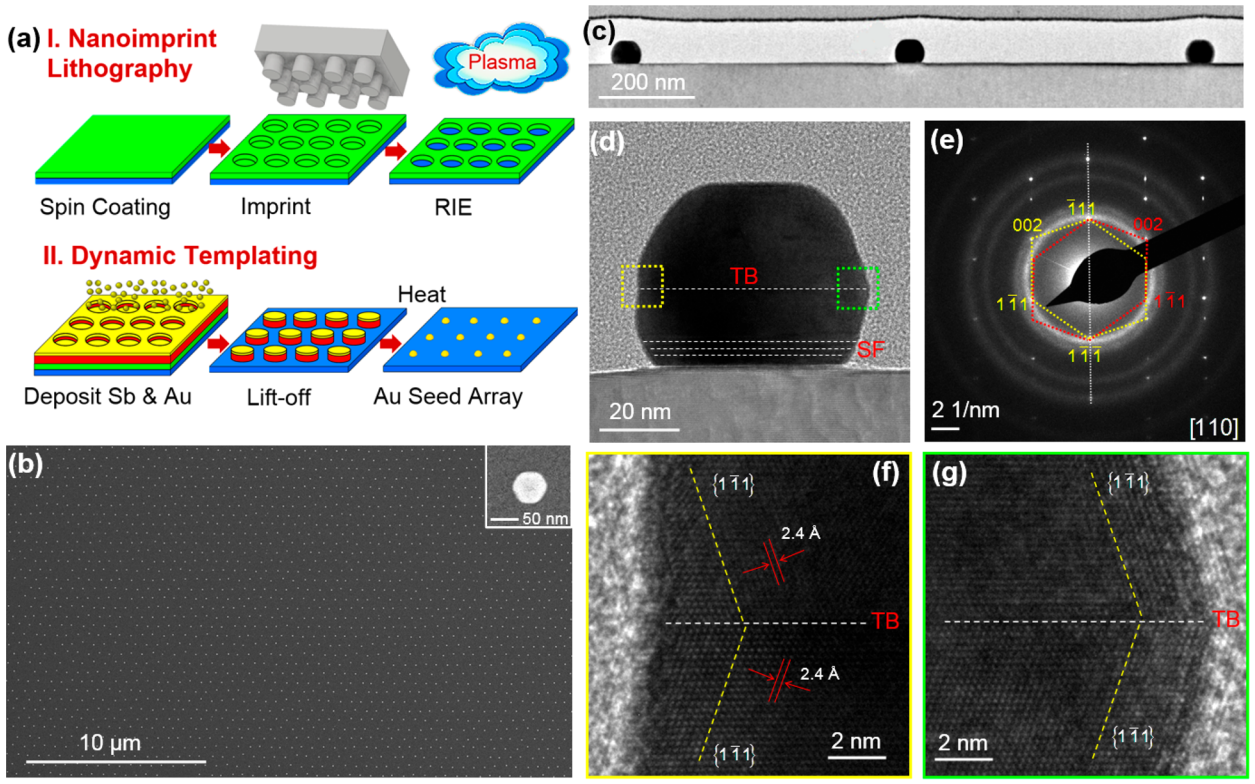

Figure 1. (a) Schematic of the processing route used to form periodic arrays of Au seeds. (b) SEM image of the array where the inset shows a magnified view of a single structure. (c) TEM image of Au seeds after FIB cross-sectioning. (d) Cross-sectional TEM image of a single Au seed, (e) SAED pattern taken along a [110] zone axis, and (f,g) HRTEM images of the areas denoted by the yellow and green boxes in Figure 1d. TB and SF are used to label prominent twin boundaries and stacking faults, respectively. The 2.4 Å spacing between the {111} planes of Au is labeled on the HRTEM image.

and subsequently grown into nanoplate geometries using wet chemistry,[23−27] these demonstrations often suffer from low yields and lack the ability to deposit seeds at predefined locations. There is, in fact, a lone demonstration where solution-grown nanoplates have been arranged in periodic arrays in which Zhou et al.[28] use capillary assembly to direct triangular nanoprisms into lithographically defined trenches formed over a square millimeter area in a polydimethylsiloxane (PDMS) resist.

Despite an overall lack of success in bringing solution-based nanoplate growth modes to the substrate surface, the use of electron-beam lithography to define organized surfaces of planar nanostructures has been one of the true triumphs in the field of plasmonics, both from the standpoint of applications[29−33] and in advancing a mechanistic understanding of complex phenomena.[34−38] The inherent disadvantage of this top-down approach is that the serial nature of the patterning process makes the fabrication of large areas time-consuming and cost-prohibitive. Nanosphere lithography, which uses close-packed colloidal spheres to form a shadow mask through which a metal is deposited,[39] alleviates this concern but suffers from restrictions on nanostructure placement and a lack of true long-range order. For all cases, the structures formed have a polycrystalline character that leads to a plasmon resonance with a lower quality factor.[40]

Recently, we demonstrated a nanofabrication route that synergistically combines nanoimprint lithography (NIL), vapor-phase directed assembly, and liquid-phase epitaxy to obtain periodic arrays of complex noble metal nanostructures over a square centimeter area.[41] This benchtop process leverages a synthetic strategy in which seed-mediated liquid-phase growth modes are carried out on substrate-immobilized seeds.[42] Although this strategy, as practiced by us and others, has led to the generation of a library of substrate-based structures with considerable architectural diversity,[43−48] it has been fundamentally limited by the inability to fabricate seeds that have the same internal defect structure as those routinely used in colloidal chemistry. Here, we demonstrate a large-area processing route for generating substrate-based Au seeds lined with stacking faults and use them to synthesize periodic arrays of epitaxially aligned Au nanoplates using a plasmon-mediated growth mode. These demonstrations represent an advancement in substrate-based noble metal nanofabrication and provide a new platform for obtaining a mechanistic understanding of plasmon-mediated syntheses.

The demands placed on the seeds needed to generate periodic arrays of Au nanoplates are far more stringent than those used in colloidal syntheses in that they must not only exhibit stacking faults but these defects must run parallel to the substrate surface. This necessitates that the seeds have their [111]-orientation normal to the substrate surface where the formation of planar defects along the other crystallographically equivalent ⟨111⟩ directions is unfavorable. The demands on the yield are also more severe because the purification of the final product through centrifugation is impossible. The seed fabrication process, which is shown schematically in Figure 1a, uses NIL in combination with a high-temperature templated-assembly process referred to as dynamic templating.[49] The NIL process utilizes a lithographically defined stamp to emboss a periodic array of cylindrical holes into a moldable polymer

DOI: 10.1021/acs.nanolett.9b02215
Nano Lett. 2019, 19, 5653−5660

resist after which the stamp is removed and openings to the substrate surface are made using reactive ion etching (RIE). The dynamic templating process begins with the sequential deposition of Sb and Au onto the imprinted polymer followed by a lift-off procedure that removes the polymer and its coating, leaving behind an array of Au−Sb pedestals. Heating the pedestal causes its areal dimensions to steadily decrease as Sb sublimates from its sides, a process that leads to the forced agglomeration of the Au atop the receding pedestal until finally the pedestal collapses and any remaining Sb is lost to the vapor phase. While such an assembly process can be carried out without using Sb, its presence allows for the assembly of arrayed nanostructures that are much smaller than otherwise possible,[49] a capability that proves essential to the synthesis of nanoplates (vide infra).

Figure 1b shows an SEM image of a periodic array of Au seeds. The seeds show faceting that is consistent with a substrate-truncated Wulff shape with its [111]-axis oriented normal to the substrate surface.[50] A histogram of the seed diameter (Figure S1a) reveals a high degree of size uniformity with an average value of 66 nm. Registration errors of 100 nm on an array pitch of 600 nm are common (Figure S1b). The Au structures show a sharp localized surface plasmon resonance (LSPR) at 550 nm (Figure S1c). TEM characterization of the seed crystallinity and internal defect structure was performed on a cross section prepared using a focused ion beam (FIB) (Figure 1c). All of the seeds examined exhibit stacking faults where some establish twin boundaries as seen in selected area electron diffraction (SAED) and high-resolution TEM (HRTEM) images (Figure 1d−g). All of these planar defects extend from one side of the seed to the other (Figure 1f,g). TEM analysis also reveals that the Au seeds form an epitaxial relationship with the [0001]-oriented sapphire substrate (Figure S2). One of the seeds examined was, however, misoriented and showed a significantly more complex internal defect structure (Figure S3).

The formation of Au nanostructures lined with planar defects is a common occurrence that is attributable to low stacking fault energies.[13] The substrate-based seeds produced in the current work are, however, unique in that the planar defects run parallel to the substrate surface even though three equivalent ⟨111⟩-directions project out of the substrate surface at 70.53° from the normal. The significance of this result is that the substrate plays a pivotal role in the defect formation that is essential to nanoplate growth modes. The implication is that substrate surfaces could, in fact, act as an important control on syntheses that is made possible through the defect engineering of seeds. Although lattice strain at the Au−substrate interface represents the most probable cause for deterministic defect formation, the use of Sb in the seed assembly process could also be a contributing factor. With the Au−Sb binary phase diagram showing a low-temperature eutectic of 360 °C, it is highly likely that a precursor to the final Au seed existed in the liquid-state. If the liquid-to-solid phase transformation occurred rapidly, then this could induce defects as is evidenced by the formation of stacking fault defects in quenched metals.[51]

The plasmon-mediated synthesis of Au nanoplates, as devised by Wei and co-workers,[12] was adapted from colloidal chemistry to the substrate-based platform as a proof-of-concept demonstration that the Au seed arrays could be used to activate planar growth modes. Figure 2a shows a schematic of their proposed growth mode as it relates to a substrate-immobilized structure. In the synthesis, the seeds are immersed

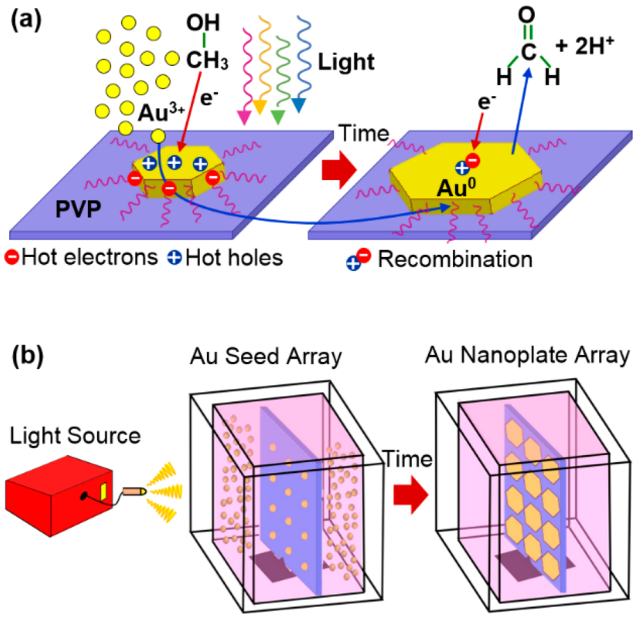

Figure 2. Schematic representations of the (a) plasmon-mediated growth mode that gives rise to Au nanoplates and (b) experimental setup used to synthesize periodic arrays of Au nanoplates using seeds with planar defects.

in a room-temperature aqueous solution of $HAuCl_4$, PVP (polyvinylpyrrolidone), and methanol. When exposed to light, the LSPR excitation generates hot electron−hole pairs. The holes are quickly scavenged by methanol (CH_3OH) in a reaction that sees it oxidized, forming formaldehyde (CH_2O) as a product. While the hot electrons are now available for the reduction of Au^{3+}, their femtosecond lifetimes are incommensurate with time scales needed for the reaction (i.e., microseconds to milliseconds).[12] An elegant means for circumventing this time scale mismatch is, however, enacted that takes advantage of the selective adsorption of PVP to the exposed planar defects on the perimeter of the Au nanostructure, a condition that has been verified using NanoSIMS (nanoscale secondary-ion mass spectrometry).[12] The PVP, which is positively charged due to the pH of the solution, acts to first attract and then prolong the lifetime of the hot electrons while simultaneously concentrating aqueous $AuCl_4^-$ at the perimeter of the nanostructure, a combination that harnesses these otherwise short-lived plasmonic excitations and, hence, provides the conditions needed for Au^{3+} reduction. It is noted that although PVP has been widely used in nanostructure synthesis[52] the role played in this plasmon-mediated growth mode is mechanistically unique. Carrying out such a synthesis on the surface of a sapphire substrate is not expected to influence this photochemistry since it has a large bandgap (E_{BG} = 9.1 eV). The substrate-based synthesis is, therefore, expected to proceed in much the same manner as the colloidal synthesis. A key difference, however, is that the seeds are immobilized on a substrate that is supported vertically in the growth solution (Figure 2b). As a result, the **E** field of the incident light, although unpolarized, is always in the direction of nanoplate growth whereas for a colloid it is time-averaged in all directions as the suspended nanostructure tumbles in the solution.

Figure 3a,b shows top- and tilted-view SEM images of the Au nanoplate array resulting from a plasmon-mediated

DOI: 10.1021/acs.nanolett.9b02215
Nano Lett. 2019, 19, 5653−5660

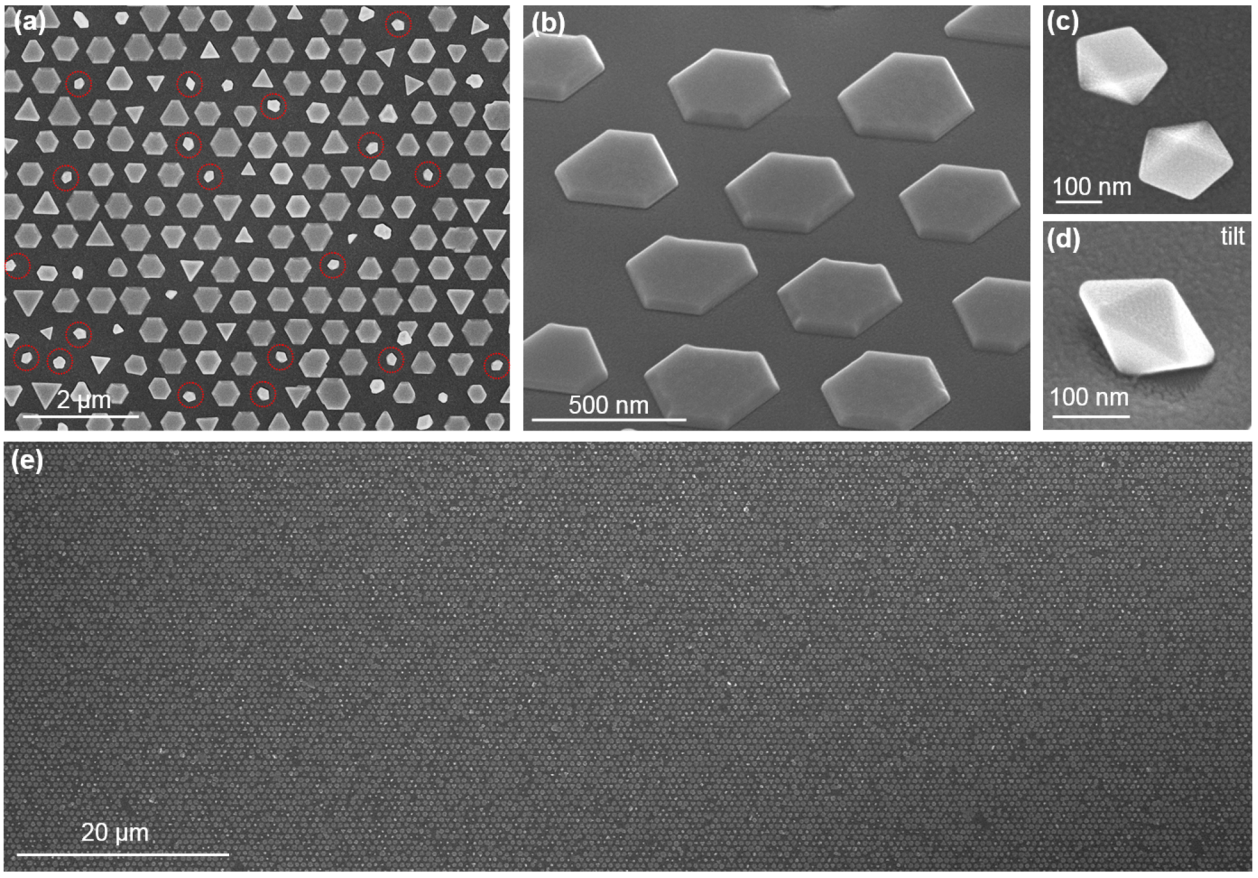

Figure 3. SEM images of the Au nanoplate array from a (a) top- and (b) tilted-view. (c) Top- and (d) tilted-view images of the decahedral nanostructures formed in low yield. The decahedral structures appearing in Figure 3a are circled in red. (e) Low-magnification image showing that the array is formed over large areas.

synthesis lasting 4 h. A statistical analysis of the nanostructure shape (Figure S4 and Table S1) reveals that 78% of the structures exhibit a nanoplate geometry where 57% are hexagonal, 11% are triangular, and 10% are corner-truncated triangles. The remaining structures exhibit a three-dimensional geometry that often shows the pentatwin pattern characteristic of decahedral nanocrystals (Figure 3c,d). Although the 78% nanoplate yield is far from optimal, it eclipses the 21% yield reported for the colloidal growth mode.[12] The higher yield further underscores the importance of the substrate in promoting the defect structures needed to facilitate nanoplate growth. Histograms of the size distributions for the various structures (Figure S5) reveal an average hexagon width of 450 nm, a triangular base width of 400 nm, and three-dimensional structure diameters of 200 nm. The thickness of the nanoplates is close to that of the seed, indicating that nearly all of the growth occurs at the perimeter of the structure. A striking feature of the surfaces produced is the in-plane alignment of the nanoplates, showing edges that run parallel to each other as well as the $(11\bar{2}0)$ plane of the sapphire substrate. This alignment provides a clear indication that the Au seeds share a heteroepitaxial relationship with the substrate. Additionally, the effectiveness of NIL in generating large areas of arrayed nanoplates is made evident by Figure 3e. A time series of spectroscopic measurements taken of an array over the course of a synthesis (Figure S6), in combination with discrete dipole approximation (DDA) simulations,[53] reveal a steadily red-shifting plasmon peak as is expected for a nanoplate growth mode[54] as well as a second peak that red shifts to a lesser degree that is associated with the three-dimensional structures.[55] These spectroscopic results are, therefore, consistent with what is observed in the SEM images. It is noted that the nanoplate architecture is stable in air for long durations but experiences a 12 nm red shift in the LSPR when exposed to deionized water for 24 h, as has been similarly observed for colloidal Au nanoplates (Figure S7).[56]

With the plasmon-mediated synthesis of Au nanoplates now demonstrated using both colloidal and substrate-immobilized seeds, comparisons can be drawn. When carried out in the dark, the substrate-based growth mode, like its colloidal counterpart,[12] resulted in drastically reduced growth rates (Figure S8a,b). Increasing the growth time from 4 to 24 h did, however, see the emergence of nanoplates (Figure S8c). The seeds used in the current study with an average diameter of 66 nm, are considerably larger than the 7 nm seeds used in the colloidal synthesis. Nanoplate growth modes, in general, tend to use small seeds because larger sizes lead to a substantial drop in yield.[1,57] The substrate-based nanoplate growth mode does, however, break down when seed diameters of 130 nm are used, yielding irregular-shaped structures with more of a three-dimensional character (Figure S9). The formation of decahedral nanocrystals is also observed in both the colloidal and substrate-based growth modes. It is, however, somewhat surprising for such a geometry to originate from these substrate-based seeds because they exist in sizes and are produced at temperatures where the pentatwinned architecture is thermodynamically unfavorable.[15,58] The fact that the decahedral structures show a consistent tilt relative to the

DOI: 10.1021/acs.nanolett.9b02215
Nano Lett. 2019, 19, 5653−5660

substrate surface (Figure 3d) suggests that seed−substrate epitaxy plays a significant role in their formation. Neither the seed nor the internal defect structure needed to promote substrate-based decahedral growth has been identified in this study.

Hexagonal and triangular nanoplates were detached from the substrate and placed on a holey carbon TEM grid using procedures outlined in the Supporting Information. Figure 4

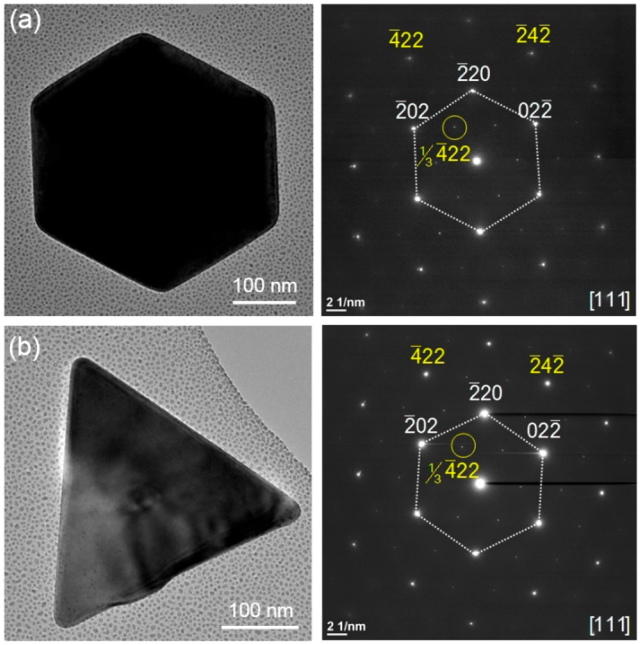

Figure 4. Plan view TEM image and its corresponding SAED pattern for a (a) hexagonal and (b) triangular nanoplate.

shows plan view TEM images of these structures and their corresponding SAED patterns. Indexing reveals the presence of the six {220} reflections expected for a [111]-oriented Au nanoplate. Also observed are six 1/3{422} reflections that are forbidden for an fcc crystal structure. Such reflections can, however, occur when stacking faults are present in the nanocrystal that run parallel to the (111) basal plane.[59] This data provides further evidence that planar defects are the primary shape-determining factor in this substrate-based growth mode.

Although it is apparent that the substrate-based nanoplate growth mode is promoted by seeds lined with planar defects, the cause of the substantial variation in nanostructure shape remains an open question. In an effort to gain insights into this variation, cross-sectional TEM was carried out where the structures selected for FIB cross-sectioning were chosen to reflect those most commonly observed. Figure 5a shows a top-view SEM image of the targeted structures (denoted by the dashed red box) as well as a TEM image of the same structures after FIB cross-sectioning. Figure 5b−e presents TEM images and SAED patterns for Au nanostructures with a hexagonal (H), triangular (T), truncated triangular (TT), and three-dimensional (3D) morphology. All of these nanocrystals show a defect-rich structure where it is evident that the seed stacking faults propagated into the emerging nanoplate as material was added to the perimeter. For all four cases, the [111]-axis of the nanostructure is perpendicular to the substrate surface where each shares the same heteroepitaxial relationship with the substrate (Figure S10b−e). Although the SAED patterns and HRTEM images all show the mirror planes that are characteristic of twin boundaries (denoted TB), the three-dimensional structure is unique in that the twin plane does not run parallel to the substrate surface but instead projects out of its surface at an angle of approximately 70° to the normal. This nanostructure, hence, displays the defects needed for nanoplate growth but with a trajectory that is away from the surface rather than running parallel to it. The fact that no nanoplate emerged could indicate that the influence of the substrate on the nanoplate growth mode extends beyond merely promoting the formation of planar defects. It is also noted that a misaligned structure with its [100]-axis perpendicular to the surface has also been observed to have planar defects but it too gave rise to a three-dimensional geometry (Figure S10f). It is, in fact, an extremely rare occurrence for a nanoplate to emerge with a growth trajectory other than one that is parallel to the substrate surface.

A comparison of the three nanoplate structures shown in Figure 5b−d reveals key differences in terms of both the side-faceting (denoted by red circles) and defect structures. In terms of side-faceting, the hexagonal nanoplate exhibits two facets whereas the triangular nanoprism has one. Although this is not surprising, an examination of the internal defect structure reveals that the hexagonal structure is especially rich in planar defects where the two facets meet near the midpoint of the structure while the triangular nanoprism has the highest density of defects near the substrate surface. The third structure, a truncated triangle, also has planar defects near the surface, but they extend over a greater vertical distance than that of the triangular nanoprism. These results suggest that the location of these highly defected regions are crucial in determining nanoplate shape. It is revealing that even the three-dimensional structure (Figure 5e) shows two facets meeting where the defect density is the largest. While it is conceded that making such a conclusion based on the examination of only a few structures is somewhat tenuous, it is corroborated by the work of Aherne et al.[60] who came to a similar conclusion for Ag nanoplates. They proposed that planar defect structures, when centrally located within the seed, lead to the formation of two equally sized facets about the midpoint of the seed that are able to effectively compete with each other during growth to form hexagonal geometries. In contrast, noncentrally located defects allow one facet to dominate growth, resulting in triangular geometries.

Prior to this study, the adaptation of seed-mediated colloidal growth modes to substrate-immobilized seeds have relied on the use of single-crystal seeds. Their use has resulted in the synthesis of cuboctahedrons,[44,45] octahedrons,[45,61] nanocubes,[47,48] tetrahexahedrons,[44] core−shell,[47,48] nanoshell,[62] core−void−shell,[46] and dimer structures.[61] By establishing a protocol for the synthesis of seeds lined with planar defects, it should prove possible to adapt other prominent colloidal Au nanoplate protocols[16,40,56,63−68] to the substrate surface. This work should also significantly expand the breadth of nanostructure architectures accessible to the substrate platform because planar structures with variable shape, a bimetallic character, and which use nanoplates as a starting template for the generation of more sophisticated structures[17−20] may now be synthetically viable. Even this initial demonstration provides an intriguing building block for device applications because Au nanoplates offer chemical inertness, biocompatibility, and a tunable plasmon resonance that extends from the visible to the

DOI: 10.1021/acs.nanolett.9b02215
Nano Lett. 2019, 19, 5653−5660

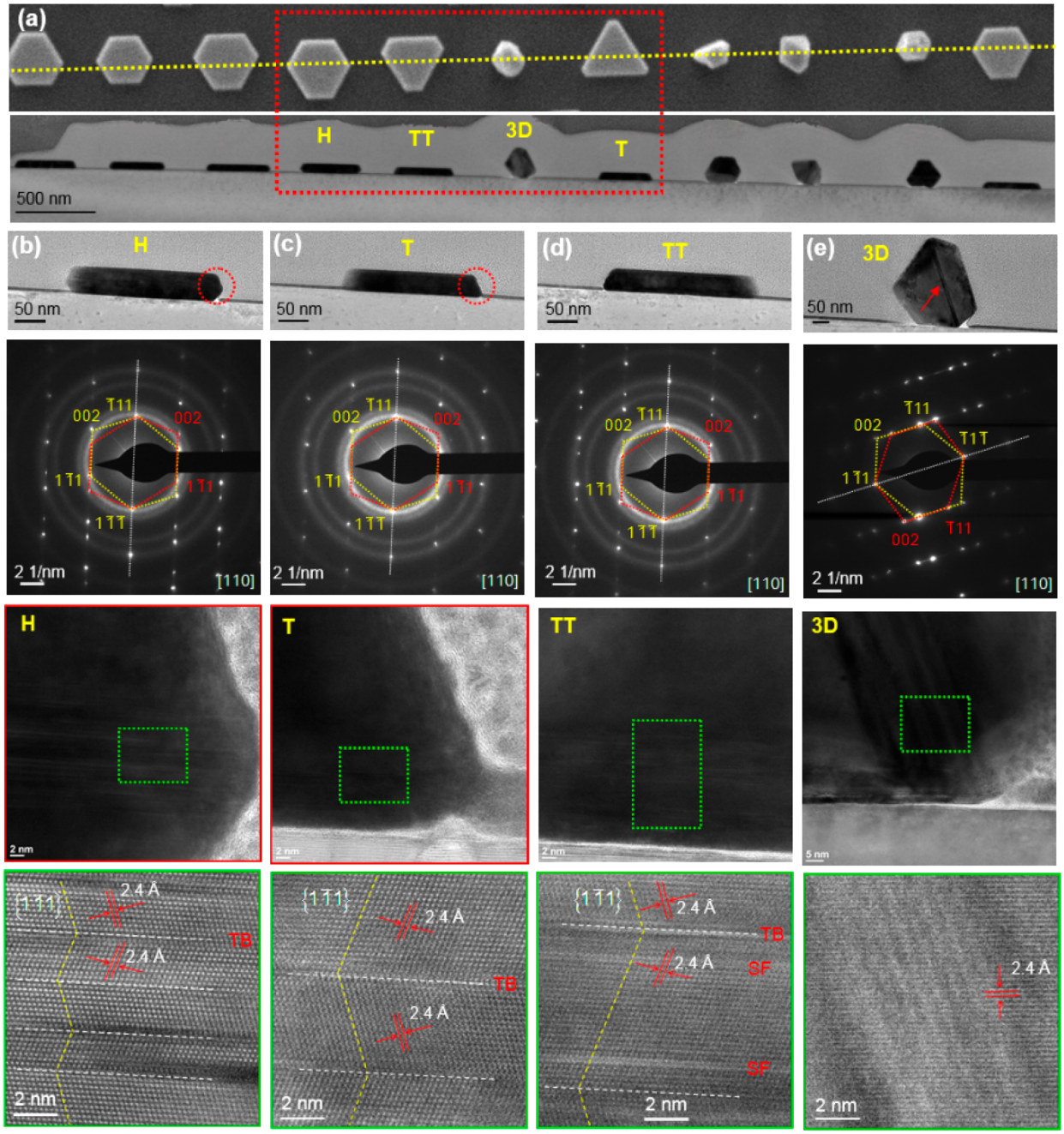

Figure 5. (a) Top- and cross-sectional view of substrate-based Au nanostructures after FIB cross-sectioning. The dashed yellow line denotes the position of the edge targeted during FIB milling. Cross-sectional TEM images, SAED patterns, and HRTEM images for nanostructures with a (b) hexagonal (H), (c) triangular (T), (d) truncated triangular (TT), and (e) three-dimensional (3D) morphology. The zone axis for each SAED pattern is shown in the bottom right corner.

infrared. Moreover, the integration of nanoplate geometries with wafer-based lithographic processes and structures is conceptually appealing in that both have a two-dimensional character. From a broader perspective, this work demonstrates the utility of using a substrate surface as the primary driver for seed nucleation events that promote specific internal defect structures and crystallographic alignments relative to the substrate surface. Challenges do, however, remain in terms of obtaining higher nanoplate yields and in improving size and shape uniformity. Encouraging is that Gilroy et al.[58] were able to systematically vary the internal defect structure of substrate-based Ag nanostructures between cuboctahedral, decahedral, and icosahedral geometries through the use of thermodynamic controls.

Another unique aspect of this study is that it represents the first plasmon-mediated synthesis to yield periodic arrays of heteroepitaxially aligned substrate-based nanoplates, a platform that provides an excellent testbed for manipulating syntheses using light as a synthetic lever[1] and for studying plasmon-mediated chemistry derived from hot electrons interacting with adsorbed species.[69] One of the most attractive features of plasmon-mediated syntheses is the ability to substantially narrow the size distribution through the use of monochromatic light.[1,10,11] This capability arises from the fact that the growth

DOI: 10.1021/acs.nanolett.9b02215
Nano Lett. 2019, 19, 5653−5660

rate is self-limiting in that it dramatically slows once the structure has grown to a size that red shifts its plasmon resonance beyond that of the excitation wavelength. If this same procedure proves adaptable to substrate-based growth modes, then it should prove possible to substantially narrow the size distribution. Substrate-based structures also lend themselves to a comprehensive examination of the role that polarized light has on plasmon-mediated growth modes. Prior studies have led to mixed results from the standpoint of determining whether polarization is a factor in shape-determination.[12,23,26,70−72] Because hot-electrons are produced in greater quantity at the sharp corners of nanostructures,[73] a coincident polarization direction could also accelerate the growth rate. Opportunities also arise in terms of altering the nanostructure shape through variations to the internal defect structure of the seed or through manipulations to the chemical environment during growth. Colloidal studies of the Au nanoplate growth mode have already shown that such manipulations can give rise to triangular nanoprisms[12] and three-dimensional Au structures with a spiral geometry.[74]

In summary, we have demonstrated the nanofabrication of periodic arrays of substrate-based seeds lined with planar defects and used them to enact a plasmon-mediated chemistry that gives rise to Au nanoplates. The process is unique in that it uses substrate-based epitaxy, nanoimprint lithography, and vapor phase assembly processes as unconventional synthetic levers that when used in tandem with well-established liquid-phase chemistry leads to the formation of organized surfaces of planar nanostructures over large areas. This work also demonstrates the utility of using a crystalline substrate as the primary driver for seed nucleation events that promote specific internal defect structures and crystallographic alignments relative to the substrate surface. With the synthesis of periodic arrays of Au nanoplates and the viability of plasmon-mediated growth modes using substrate-immobilized seeds now demonstrated, this study lays the foundation for new synthetic strategies, presents a unique platform for mechanistic studies, and provides an attractive new building block for the design of photoactive surfaces.

■ ASSOCIATED CONTENT

Supporting Information

The Supporting Information is available free of charge on the ACS Publications website at DOI: 10.1021/acs.nanolett.9b02215.

Experimental details and additional data (PDF)

■ AUTHOR INFORMATION

Corresponding Author

*E-mail: sneretina@nd.edu (S.N.).

ORCID

Svetlana Neretina: 0000-0002-6889-4384

Notes

The authors declare no competing financial interest.

■ ACKNOWLEDGMENTS

This work is supported by a National Science Foundation Award (DMR-1803917). It has also benefited from the facilities available through the Notre Dame Integrated Imaging Facility (NDIIF). The authors are grateful to and acknowledge the expertise of Tatyana Orlova in the preparation of the TEM cross sections.

■ REFERENCES

(1) Langille, M. R.; Personick, M. L.; Mirkin, C. A. *Angew. Chem., Int. Ed.* **2013**, *52*, 13910−13940.
(2) Tan, C.; Qin, C.; Sadtler, B. *J. Mater. Chem. C* **2017**, *5*, 5628−5642.
(3) Millstone, J. E.; Hurst, S. J.; Métraux, G. S.; Cutler, J. I.; Mirkin, C. A. *Small* **2009**, *5*, 646−664.
(4) Pastoriza-Santos, I.; Liz-Marzán, L. M. *J. Mater. Chem.* **2008**, *18*, 1724−1737.
(5) Jin, R.; Cao, Y.; Mirkin, C. A.; Kelly, K. L.; Schatz, G. C.; Zheng, J. G. *Science* **2001**, *294*, 1901−1903.
(6) Xue, C.; Métraux, G. S.; Millstone, J. E.; Mirkin, C. A. *J. Am. Chem. Soc.* **2008**, *130*, 8337−8344.
(7) Wu, X.; Redmond, P. L.; Liu, H.; Chen, Y.; Steigerwald, M.; Brus, L. *J. Am. Chem. Soc.* **2008**, *130*, 9500−9506.
(8) Zheng, X.; Xu, W.; Corredor, C.; Xu, S.; An, J.; Zhao, B.; Lombardi, J. R. *J. Phys. Chem. C* **2007**, *111*, 14962−14967.
(9) Jin, R.; Cao, C. Y.; Hao, E.; Metraux, G. S.; Schatz, G. C.; Mirkin, C. A. *Nature* **2003**, *425*, 487−490.
(10) Callegari, A.; Tonti, D.; Chergui, M. *Nano Lett.* **2003**, *3*, 1565−1568.
(11) Maillard, M.; Huang, P.; Brus, L. *Nano Lett.* **2003**, *3*, 1611−1615.
(12) Zhai, Y.; DuChene, J. S.; Wang, Y.-C.; Qiu, J.; Johnston-Peck, A. C.; You, B.; Guo, W.; DiCiaccio, B.; Qian, K.; Zhao, E. W.; Ooi, F.; Hu, D.; Su, D.; Stach, E. A.; Zhu, Z.; Wei, W. D. *Nat. Mater.* **2016**, *15*, 889−893.
(13) Xia, Y.; Gilroy, K. D.; Peng, H. C.; Xia, X. *Angew. Chem., Int. Ed.* **2017**, *56*, 60−95.
(14) Wang, H.; Zhou, S.; Gilroy, K. D.; Cai, Z.; Xia, Y. *Nano Today* **2017**, *15*, 121−144.
(15) Zhou, S.; Zhao, M.; Yang, T. H.; Xia, Y. *Mater. Today* **2019**, *22*, 108−131.
(16) Ni, Y.; Kan, C.; Xu, J.; Liu, Y. *Superlattices Microstruct.* **2018**, *114*, 124−142.
(17) Chen, Y.; Fan, Z.; Zhang, Z.; Niu, W.; Li, C.; Yang, N.; Chen, B.; Zhang, H. *Chem. Rev.* **2018**, *118*, 6409−6455.
(18) Nasilowski, M.; Mahler, B.; Lhuillier, E.; Ithurria, S.; Dubertret, B. *Chem. Rev.* **2016**, *116*, 10934−10982.
(19) Fan, Z.; Huang, X.; Tan, C.; Zhang, H. *Chem. Sci.* **2015**, *6*, 95−111.
(20) Hu, H.; Zhou, J.; Kong, Q.; Li, C. *Part. Part. Syst. Charact.* **2015**, *32*, 796−808.
(21) Liebig, F.; Sarhan, R. M.; Sander, M.; Koopman, W.; Schuetz, R.; Bargheer, M.; Koetz, J. *ACS Appl. Mater. Interfaces* **2017**, *9*, 20247−20253.
(22) Scarabelli, L.; Coronado-Puchau, M.; Giner-Casares, J. J.; Langer, J.; Liz-Marzán, L. M. *ACS Nano* **2014**, *8*, 5833−5842.
(23) Paul, A.; Kenens, B.; Hofkens, J.; Uji-I, H. *Langmuir* **2012**, *28*, 8920−8925.
(24) Beeram, S. R.; Zamborini, F. P. *ACS Nano* **2010**, *4*, 3633−3646.
(25) Umar, A. A.; Oyama, M.; Salleh, M. M.; Majlis, B. Y. *Cryst. Growth Des.* **2009**, *9*, 2835−2840.
(26) Redmond, P. L.; Wu, X.; Brus, L. *J. Phys. Chem. C* **2007**, *111*, 8942−8947.
(27) Umar, A. A.; Oyama, M. *Cryst. Growth Des.* **2006**, *6*, 818−821.
(28) Zhou, Y.; Zhou, X.; Park, D. J.; Torabi, K.; Brown, K. A.; Jones, M. R.; Zhang, C.; Schatz, G. C.; Mirkin, C. A. *Nano Lett.* **2014**, *14*, 2157−2161.
(29) Wang, W.; Ramezani, M.; Väkeväinen, A. I.; Törmä, P.; Rivas, J. G.; Odom, T. W. *Mater. Today* **2018**, *21*, 303−314.
(30) Dong, L.; Yang, X.; Zhang, C.; Cerjan, B.; Zhou, L.; Tseng, M. L.; Zhang, Y.; Alabastri, A.; Nordlander, P.; Halas, N. J. *Nano Lett.* **2017**, *17*, 5768−5774.
(31) Fritzsche, J.; Albinsson, D.; Fritzsche, M.; Antosiewicz, T. J.; Westerlund, F.; Langhammer, C. *Nano Lett.* **2016**, *16*, 7857−7864.

DOI: 10.1021/acs.nanolett.9b02215
Nano Lett. 2019, 19, 5653−5660

(32) Zhang, C.; Zhao, H.; Zhou, L.; Schlather, A. E.; Dong, L.; McClain, M. J.; Swearer, D. F.; Nordlander, P.; Halas, N. J. *Nano Lett.* **2016**, *16*, 6677−6682.
(33) Chang, W.-S.; Lassiter, J. B.; Swanglap, P.; Sobhani, H.; Khatua, S.; Nordlander, P.; Halas, N. J.; Link, S. *Nano Lett.* **2012**, *12*, 4977−4982.
(34) Baumberg, J. J.; Aizpurua, J.; Mikkelsen, M. H.; Smith, D. R. Extreme Nanophotonics from Ultrathin Metallic Gaps. *Nat. Mater.* **2019**, *18*, 668−678.
(35) Tumkur, T.; Yang, X.; Zhang, C.; Yang, J.; Zhang, Y.; Naik, G. V.; Nordlander, P.; Halas, N. J. *Nano Lett.* **2018**, *18*, 2040−2046.
(36) Knight, M. W.; King, N. S.; Liu, L.; Everitt, H. O.; Nordlander, P.; Halas, N. J. *ACS Nano* **2014**, *8*, 834−840.
(37) Duan, H.; Hu, H.; Kumar, K.; Shen, Z.; Yang, J. K. W. *ACS Nano* **2011**, *5*, 7593−7600.
(38) Wang, D.; Koh, Y. R.; Kudyshev, Z. A.; Maize, K.; Kildishev, A. V.; Boltasseva, A.; Shalaev, V. M.; Shakouri, A. *Nano Lett.* **2019**, *19*, 3796−3803.
(39) Haynes, C. L.; Van Duyne, R. P. *J. Phys. Chem. B* **2001**, *105*, 5599−5611.
(40) Viarbitskaya, S.; Teulle, A.; Marty, R.; Sharma, J.; Girard, C.; Arbouet, A.; Dujardin, E. *Nat. Mater.* **2013**, *12*, 426−432.
(41) Menumerov, E.; Golze, S. D.; Hughes, R. A.; Neretina, S. *Nanoscale* **2018**, *10*, 18186−18194.
(42) Neretina, S.; Hughes, R. A.; Gilroy, K. D.; Hajfathalian, M. *Acc. Chem. Res.* **2016**, *49*, 2243−2250.
(43) Hughes, R. A.; Menumerov, E.; Neretina, S. *Nanotechnology* **2017**, *28*, 282002.
(44) Preston, A. S.; Hughes, R. A.; Demille, T. B.; Rey Davila, V. M.; Neretina, S. *Acta Mater.* **2019**, *165*, 15−25.
(45) Perez Cardenas, M. T.; Kong, C.; He, J.; Litvin, S.; Meyerson, M. L.; Nie, Z. *ACS Nano* **2018**, *12*, 1107−1119.
(46) Hajfathalian, M.; Gilroy, K. D.; Golze, S. D.; Yaghoubzade, A.; Menumerov, E.; Hughes, R. A.; Neretina, S. *ACS Nano* **2016**, *10*, 6354−6362.
(47) Hajfathalian, M.; Gilroy, K. D.; Hughes, R. A.; Neretina, S. *Small* **2016**, *12*, 3444−3452.
(48) Liu, G.; Zhang, C.; Wu, J.; Mirkin, C. A. *ACS Nano* **2015**, *9*, 12137−12145.
(49) Farzinpour, P.; Sundar, A.; Gilroy, K. D.; Eskin, Z. E.; Hughes, R. A.; Neretina, S. *Nanoscale* **2013**, *5*, 1929−1938.
(50) Henry, C. R. *Prog. Surf. Sci.* **2005**, *80*, 92−116.
(51) Robach, J. S.; Robertson, I. M.; Lee, H. J.; Wirth, B. D. *Acta Mater.* **2006**, *54*, 1679−1690.
(52) Koczkur, K. M.; Mourdikoudis, S.; Polavarapu, L.; Skrabalak, S. E. *Dalton Trans* **2015**, *44*, 17883−17905.
(53) Draine, B. T.; Flatau, P. J. *J. Opt. Soc. Am. A* **1994**, *11*, 1491−1499.
(54) Ah, C. S.; Yun, Y. J.; Park, H. J.; Kim, W.-J.; Ha, D. H.; Yun, W. S. *Chem. Mater.* **2005**, *17*, 5558−5561.
(55) Malikova, N.; Pastoriza-Santos, I.; Schierhorn, M.; Kotov, N. A.; Liz-Marzan, L. M. *Langmuir* **2002**, *18*, 3694−3697.
(56) Qin, F.; Zhao, T.; Jiang, R.; Jiang, N.; Ruan, Q.; Wang, J.; Sun, L.-D.; Yan, C.-H.; Lin, H.-Q. *Adv. Opt. Mater.* **2016**, *4*, 76−85.
(57) Xue, C.; Millstone, J. E.; Li, S.; Mirkin, C. A. *Angew. Chem., Int. Ed.* **2007**, *46*, 8436−8439.
(58) Gilroy, K. D.; Puibasset, J.; Vara, M.; Xia, Y. *Angew. Chem., Int. Ed.* **2017**, *56*, 8647−8651.
(59) Germain, V.; Li, J.; Ingert, D.; Wang, Z. L.; Pileni, M. P. *J. Phys. Chem. B* **2003**, *107*, 8717−8720.
(60) Aherne, D.; Ledwith, D. M.; Gara, M.; Kelly, J. M. *Adv. Funct. Mater.* **2008**, *18*, 2005−2016.
(61) Gilroy, K. D.; Hughes, R. A.; Neretina, S. *J. Am. Chem. Soc.* **2014**, *136*, 15337−15345.
(62) Gilroy, K. D.; Farzinpour, P.; Sundar, A.; Tan, T.; Hughes, R. A.; Neretina, S. *Nano Res.* **2013**, *6*, 418−428.
(63) Geng, X.; Roth, K. L.; Freyman, M. C.; Liu, J. Z.; Grove, T. Z. *Chem. Commun.* **2016**, *52*, 9829−9832.
(64) Chen, L.; Ji, F.; Xu, Y.; He, L.; Mi, Y.; Bao, F.; Sun, B.; Zhang, X.; Zhang, Q. *Nano Lett.* **2014**, *14*, 7201−7206.
(65) Kan, C.; Wang, C.; Li, H.; Qi, J.; Zhu, J.; Li, Z.; Shi, D. *Small* **2010**, *6*, 1768−1775.
(66) Miranda, A.; Malheiro, E.; Skiba, E.; Quaresma, P.; Carvalho, P. A.; Eaton, P.; de Castro, B.; Shelnutt, J. A.; Pereira, E. *Nanoscale* **2010**, *2*, 2209−2216.
(67) Millstone, J. E.; Métraux, G. S.; Mirkin, C. A. *Adv. Funct. Mater.* **2006**, *16*, 1209−1214.
(68) Millstone, J. E.; Park, S.; Shuford, K. L.; Qin, L.; Schatz, G. C.; Mirkin, C. A. *J. Am. Chem. Soc.* **2005**, *127*, 5312−5313.
(69) Zhang, Y.; He, S.; Guo, W.; Hu, Y.; Huang, J.; Mulcahy, J. R.; Wei, W. D. *Chem. Rev.* **2018**, *118*, 2927−2954.
(70) He, Y.; Cheng, Y.; Zhao, J.; Li, X.-Z.; Gong, Q.; Lu, G. *J. Phys. Chem. C* **2016**, *120*, 16954−16959.
(71) Violi, I. L.; Gargiulo, J.; von Bilderling, C.; Cortés, E.; Stefani, F. D. *Nano Lett.* **2016**, *16*, 6529−6533.
(72) Kim, N. H.; Meinhart, C. D.; Moskovits, M. *J. Phys. Chem. C* **2016**, *120*, 6750−6755.
(73) Besteiro, L. V.; Kong, X. T.; Wang, Z.; Hartland, G.; Govorov, A. O. *ACS Photonics* **2017**, *4*, 2759−2781.
(74) Zhai, Y.; Zhang, F.; Zhang, B.; Gao, X. *Adv. Mater.* **2017**, *29*, 1703102.

DOI: 10.1021/acs.nanolett.9b02215
Nano Lett. 2019, 19, 5653−5660